THE INFLUENCE OF CALCINATION TEMPERATURE ON THE STRUCTURE AND VISIBLE LIGHT PHOTOCATALYSIS PERFORMANCE OF MN–TIO_2-LOADED WOODEN ACTIVATED CARBON FIBERS

Binqing Sun
Lecturer
E-mail: sunbinqing@tust.edu.cn

Yin Chen
Postgraduate
E-mail: chenyin880828@163.com

*Xiaojun Ma**
Professor
College of Packaging & Printing Engineering
Tianjin University of Science & Technology
Tianjin 300222, China
E-mail: mxj75@tust.edu.cn

(Received April 2017)

Abstract. Mn–TiO_2-loaded wooden activated carbon fibers (Mn/TiO_2-WACF) were prepared through sol–gel and impregnation methods and characterized by X-ray diffractometer, scanning electron microscope, Fourier transform IR spectrometer, and automatic adsorption apparatus to observe the influence of load calcination temperature on its morphological structure and visible light photocatalysis performance. Results showed that Mn doping elevated the phase transformation temperature (650-750°C) of TiO_2 in Mn/TiO_2-WACF; the particle size of anatase TiO_2 in the sample gradually enlarged with the increase of calcination temperature. The N_2 adsorbing quantity of Mn/TiO_2-WACF sample initially increased and then decreased as calcination temperature increased, and 650°C became the turning point of its N_2 adsorbing quantity. The degradation methylene blue solution for Mn/TiO_2-WACF sample under visible light gradually decreased with the increase of calcination temperature, and the methylene blue solution degradation by the sample obtained under 450°C calcination temperature reached 93%.

Keywords: Wooden activated carbon fiber, TiO_2, Mn doping, Calcination temperature, Specific surface area and aperture, Visible light photocatalysis.

INTRODUCTION

As a major water consumer, the printing and dyeing industry occupies 80-90% of the wastewater quantity of the total water consumption; it also belongs to the difficult disposition of industrial wastewater, which brings serious burden on the environment. As a commonly used macromolecular basic dyestuff, methylene blue has always been considered as a target pollutant by researchers in simulation experiment of wastewater degradation in vial laboratories (Li et al 2008; Ma et al 2014a). Traditional chemical precipitation method and gas flotation method have poor effects and face serious challenges (Tanaka et al 2000; Baban et al 2003). In recent years, TiO_2 semiconductor photocatalysis technology has developed rapidly; it has also been evaluated as an ideal photocatalyst by scholars and has become a research emphasis of wastewater disposal technology by virtue of its various advantages, such as stable physical–chemical properties, strong redox capacity, high efficiency and nontoxicity, mild reaction conditions, and degradation of organic matters into CO_2 and H_2O. However, the band gap (3.2 eV) of anatase

* Corresponding author

TiO_2 is large, and only limited UV lights ($\leq$387 nm) can excite electron transition, which results in insufficient exertion of photocatalysis (Tanaka et al 2000; Baban et al 2003; Chen and Mao 2007). Moreover, the electron–hole pair recombination that occurs during the photocatalytic process of TiO_2 for photocatalytic effect is insufficient. Conversely, used TiO_2 powder is faced with plight, making it difficult to be recycled from the liquid reaction system. Therefore, the modified TiO_2 photocatalysis material has become a research interest. In recent years, scholars have found that the transition metal ion doping technology can realize TiO_2 modification (Fu et al 2004; Li et al 2006; Gong et al 2012). For example, after Co doping into the TiO_2 membrane, the band gap of TiO_2 was narrowed from 3.1 to 2.8 eV (Subramanian et al 2008). However, few research on Mn–TiO_2 photocatalysis effect is available (Wang et al 2009; Naeem and Feng 2010).

In the present study, a Mn–TiO_2-loaded wooden activated carbon fiber (Mn/TiO_2-WACF) photocatalysis composite material was prepared by considering the WACF as a carrier and adopting the sol–gel and impregnation methods (Li and Ma 2013; Ma et al 2014b). Scanning electron microscope (SEM), X-ray diffractometer (XRD), Fourier transformation IR (FTIR) spectrometer, and specific surface area and apertometer were used to observe the influence of load calcination temperature on the morphological structure and visible light photocatalysis performance of the Mn/TiO_2-WACF composite material.

MATERIALS AND METHODS

Materials

10.2 g of butyl titanate was weighed and slowly poured into 90 mL of absolute ethyl alcohol under violent stirring. The solution noted as A, which was colorless and transparent, was placed into a magnetic stirring for 30 min. Then, 2.182 g of distilled water and 2 mL of glacial acetic acid were successively poured into 60 mL of absolute ethyl alcohol; this solution was dissolved in 3-mL $MnSO_4 \cdot H_2O$ solution with a concentration of 17 g/L, thereby obtaining solution B. Solution B was slowly poured into solution A under constant stirring and was then left to stand and age under a constant temperature of 40°C for a certain period. A yellowish emulsion colloid, Mn–TiO_2 gel, was obtained.

A certain amount of self-made WACF was evenly immersed into a colloid, which had been successfully prepared. The solution was taken out after vibration and left standing for 30 min. It was then placed into a vacuum tube-type stove after the drying process under 105°C for 1 h. Mn/TiO_2-WACF photocatalysis composite material was prepared after heat treatment for a certain period under different calcination temperatures through N_2 with a flow rate of 100 mL/min. The calcination temperatures of the five samples were set as 450, 550, 650, 750, and 850°C.

Characterization of the Composite Material

SEM analysis. JSM-7500F cold field emission SEM with a resolution of 3.0 nm and acceleration voltage of 1 kV was adopted to characterize the appearance and morphology diagrams of the samples. After Mn/TiO_2-WACF photocatalysis composite material samples were placed into the drying process, they were bonded on the sample table to conduct surface vacuum metal spraying and observe their surface morphologies.

XRD analysis. D/Max 2500 XRD (RIGAKU) was adopted to measure the XRD spectral diagram of the samples. The Cu Kα ray used was $\lambda = 1.5405$ nm, the tube voltage was 40 kV, the tube current was 100 mA, the scanning angle scope 2θ was 20-80°, and the scanning speed was 8° min^{-1}.

According to Scherrer formula,

$$D = \frac{K_1 \lambda}{\beta_{1/2} \cos\theta}. \quad (1)$$

where D (nm) is the average diameter of TiO_2 in the photocatalysis samples, K_1 is the shape factor of the crystalline with a value of 0.89, λ is the

wavelength of the X-ray with a value of 0.154 nm, $\beta_{1/2}$ is the full width at half maximum of the diffraction peak (rad), and θ is the diffraction angle (°).

$$X_A = \frac{I_A}{(I_A + 1.265/I_R)} \quad (2)$$

Eq 2 calculates the X_A content of the anatase TiO_2, where I_A is the peak intensity of the anatase crystal form (101 planes), and I_R is the peak intensity of the rutile crystal form (110 planes).

FTIR analysis. Nicolet 6700 FTIR (U.S. Thermo Electron Corporation) was adopted to measure the samples and obtain IR spectrum diagrams. The samples were tested through 1:300 KBr disc technique, with a scanning time of 32, resolution of 4 cm^{-1}, and scanning range of 400-4000 cm^{-1}.

Specific Surface Area and Aperture Analysis

ASAP-2020 automatic adsorption apparatus (U.S. Micromeritics Instrument Corporation) was used to measure the samples and obtain their adsorption isotherms. N_2 was used as the adsorbate, and the adsorption was implemented under liquid–nitrogen temperature at 77 K. According to the obtained adsorption isotherms, the Brunauer-Emmett-Teller (BET) and *t*-plot methods were used to calculate the specific surface area and the micropore specific surface area and micropore volume of the samples, respectively; the Horvath-Kawazoe (HK) and Barrett-Joyner-Halenda (BJH) methods were used to calculate the micropore and mesopore diameter distributions, respectively.

Photocatalysis Performance Test

A 33-mg methylene blue medicine was weighed and dissolved in 1000 mL of distilled water at 60°C and was then placed in a volumetric flask for standby application. 10-mg Mn/TiO_2-WACF prepared under different calcination temperatures was accurately weighed and then placed in a beaker with 100 mL of methylene blue solution with a concentration of 33 mg/L. The solutions were placed in a black case and violently stirred by a magnetic stirrer for 40 min until it reached adsorption equilibrium. A UV-1600 spectrophotometer (Shanghai MAPADA Instrument Co., Ltd, Shanghai, China) was used to measure and record absorbance A_0 in the preliminary test under a wavelength of 665 nm. The beakers filled with samples were covered by 400-800 nm optical filters. Under the conditions of illumination and magnetic stirring, absorbance was measured every other 40 min using a spectrophotometer, and the decolorization ratio *D* was calculated as follows:

$$D = \frac{A_0 - A}{A_0} \times 100\%, \quad (3)$$

where A_0 is the solution absorbance before illuminance, and *A* is the solution absorbance at one time.

RESULTS AND DISCUSSION

SEM Analysis

Figure 1 shows the SEM diagrams of the WACF and Mn/TiO_2-WACF samples. Mn–TiO_2 was evenly dispersed onto the WACF surface and presented an anomaly and discontinuous lamelliform. Figure 1b and d show that the film thickness of a single-loaded material photocatalysis at 450°C calcination temperature was at the nanometer level, thereby making WACF form a good composite structure with Mn–TiO_2. In addition, bare base materials existed on the WACF surface, which had reserved abundant pore structures and provided advantages for subsequent adsorption and photocatalysis reaction.

XRD Analysis

Figure 2 shows the XRD spectral diagrams of the Mn/TiO_2-WACF materials prepared under five different calcination temperatures. The diffraction peaks of the (101), (004), and (200) crystal planes of TiO_2 anatase phase when 2θ were 25.3, 38, and 48°, respectively, and those of the (110), (101), and (111) crystal planes of TiO_2 rutile phase when 2θ

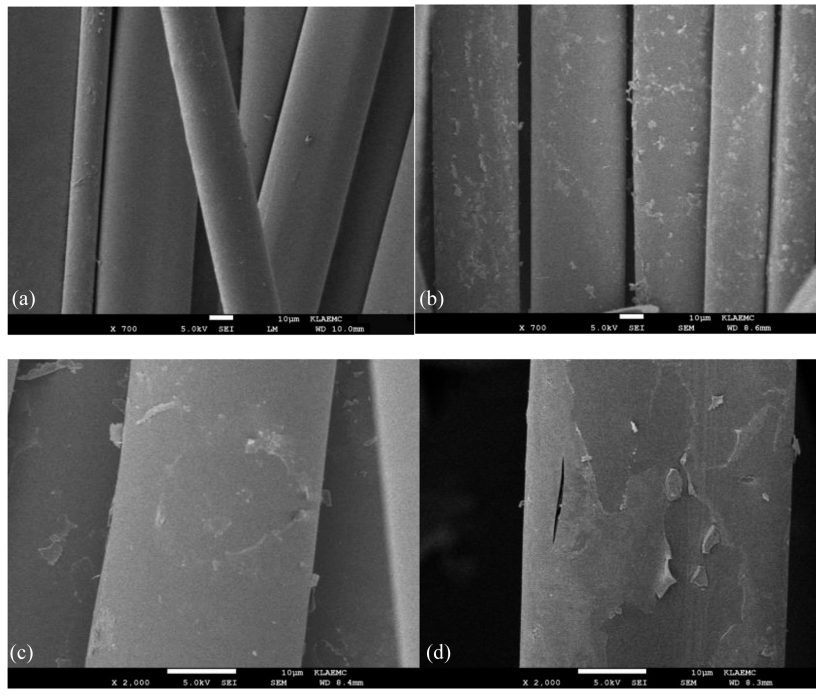

Figure 1. Scanning electron microscope diagrams of the (a) wooden activated carbon fibers (WACF) and (b-d) Mn/TiO_2-WACF samples at 450°C calcination temperature.

were 27.4, 36.1, and 41.2°, respectively. The TiO_2 composition in the Mn–TiO_2 photocatalysis composite material under 450, 550, and 650°C calcination process belonged to the anatase type, whereas the samples under the 750°C calcination process contained anatase and rutile types, in which the anatase type occupied about 10%. All TiO_2 in the sample under 850°C calcination process contained rutile crystal forms. The Mn/TiO_2-WACF samples started at the crystal phase change at 650-750°C, and the TiO_2 prepared using the sol–gel method started at approximately 550-650°C. This finding indicates that Mn doping was good for improving the heat resistance stability of the TiO_2 anatase.

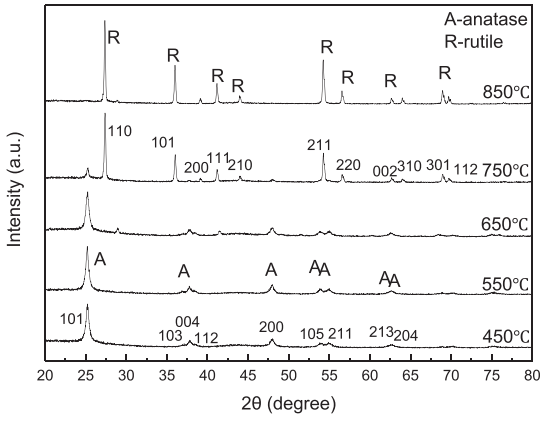

Figure 2. X-ray diffractometer diagrams of the Mn/TiO_2-wooden activated carbon fibers (WACF) samples under different calcination temperatures.

Table 1 shows the average particle size and content of anatase TiO_2 in the samples prepared under different calcination temperatures, which were calculated using Eqs 1 and 2. Before the anatase transformation occurred when the calcination temperature was between 450 and 650°C, the variations of calcination temperature had little effect on the TiO_2 particle size in the sample, and the average particle size remained at approximately 27 nm. When calcination temperature was within 650-850°C, the average particle size of TiO_2 had an increasing tendency with the

Table 1. Relationship between the calcination temperature and particle size of anatase TiO_2 in the Mn/TiO_2-wooden activated carbon fibers (WACF) samples.

Calcination temperature/°C	450	550	650	750	850
Average particle size (D(101))/nm	27	26	27	47	—
Anatase content (%)	100	100	100	10	0

increase of calcination temperature. Because of the unstable nature of anatase in the process of high-temperature treatment, the crystal phase transformation easily occurred. Meanwhile, anatase was transformed into rutile phase, which had stable and easy agglomeration, thus exerting influence on the particle size.

FTIR Analysis

The FTIR spectrum of the WACF and Mn/TiO_2-WACF samples after heat treatment under 450-850°C is shown in Fig 3. At different calcination temperatures, the IR spectrum of the Mn/TiO_2-WACF sample did not significantly change. With the increase of calcination temperature, −OH stretching vibration peak intensity within 3200-3650 cm^{-1} of the sample initially decreased and then increased, which indicated that the calcination temperature influenced the number of hydroxide radicals in the photocatalysis composite material and played a significant role in the TiO_2 photocatalysis activity (Fox and Dulay 1993). IR absorption peaks around 879, 847, and 621 cm^{-1} in the WACF were produced by the C–H bending vibration in the aromatic ring, whereas IR absorption peaks in the Mn/TiO_2-WACF were produced by the combination of Ti–O–Ti stretching and bending vibrations and C–H out-of-plane bending vibration. With the increase of calcination temperature increased, the intensity of 879 cm^{-1} absorption peak initially increased and then decreased. When calcination temperature was <750°C, all TiO_2 contained anatase and only contained rutile at 850°C.

Specific Surface Area, Pore Volume, and Aperture Analysis

Figure 4 shows the adsorption/desorption isotherms of the WACF and Mn/TiO_2-WACF at different calcination temperatures. All the adsorption/desorption isotherms of the WACFs before and after loading belonged to the typical type-I adsorption isotherms and their variation

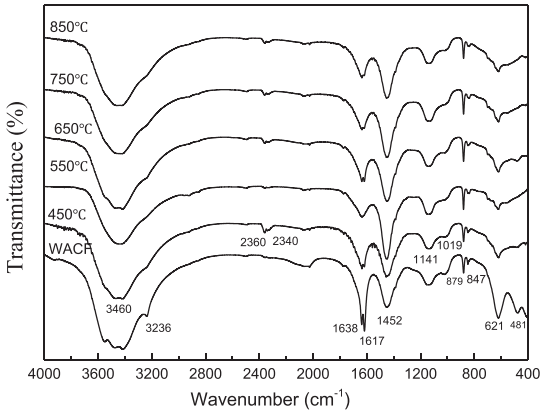

Figure 3. Fourier transformation IR spectrum of the wooden activated carbon fibers (WACF) and Mn/TiO_2-WACF samples with different calcination temperatures.

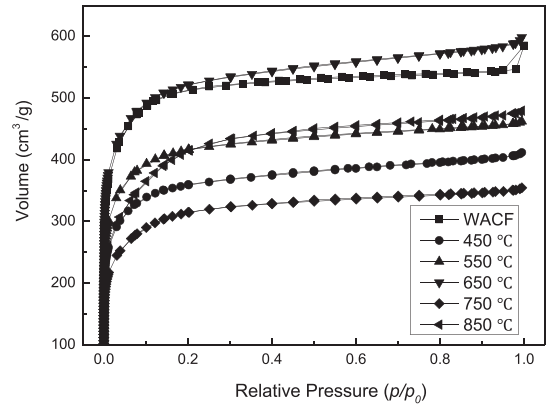

Figure 4. N_2 adsorption/desorption isotherm of the Mn/TiO_2-wooden activated carbon fibers (WACF) samples at different calcination temperatures.

tendencies were similar. Carrier fiber and Mn/TiO_2-WACF at 650°C experienced obvious hangover boosting phenomena and belonged to the type I-B material. This result indicated an uneven particle distribution or the appearance of some mesopores and macropores. Other materials belonged to the type I-A. The N_2 adsorption quantity of the Mn/TiO_2-WACF calcinated below 650°C gradually increased with the increase of calcination. When calcination temperature increased from 650 to 750°C, the N_2 adsorption quantity abruptly decreased because of the anatase–rutile phase transformation of the photocatalyst TiO_2 in Mn/TiO_2-WACF sample that occurred at 650°C. This result indicated that N_2 adsorption quantity was influenced by the crystal form variation of the photocatalyst TiO_2. Moreover, the N_2 adsorption quantity of the unloaded WACF sample was higher than that of the Mn/TiO_2-WACF sample because the Mn–TiO_2 photocatalyst had filled some pores on the surface of the carrier fiber WACF to a certain degree.

Table 2 shows the specific surface area, pore volume, and pore radius measured using the N_2 adsorption method of the Mn/TiO_2-WACF and WACF samples. Except the calcination temperatures at 650°C, specific surface area and pore volume of Mn/TiO_2-WACF samples at other temperatures were lower than those of WACF. For Mn/TiO_2-WACF samples prepared at the calcination temperatures of 450-650°C, the S_{BET}, S_{mic}, S_{meso}, V_{tot}, V_{micro}, and V_{meso} increased with the increase of calcination temperature, which indicated that the higher treatment temperature would have the better effect of fiber carrier realizing secondary pore-creating. But they would decrease at 750°C because at the moment, stability of anatase TiO_2 was damaged by high temperature, and a large quantity of rutile appeared. TiO_2 crystal phase transformation would influence particle size and agglomeration degree of photocatalyst and then affecting surface area and pore volume of fiber. Ratios of micropore volume and meshpore volume of all Mn/TiO_2-WACF samples would firstly increase and then decrease as calcination temperature increased because the loading process conduced the second calcination of fiber. Under high-temperature conditions, the fiber was conducted the second activation by CO_2 and H_2O gases formed by the carbonization of organic matters which were volatilized by Mn-TiO_2 precursor. And at calcination temperature below 550°C, higher temperature was more beneficial for the micropores formation of activated carbon fiber, whereas higher temperature above 550°C was more beneficial for the formation of activated carbon fiber mesopores.

Figure 5 shows the pore diameter distribution diagram of the WACF and Mn/TiO_2-WACF under different calcination temperatures. All samples contained submicropore, micropore, and mesopore with pore diameters between 0.5 and 3.0 nm, which indicated that the loaded Mn-TiO_2 had no influence on the pore diameter distribution of the carrier fiber. A weak new peak appeared at 0.65 nm of the sample at <850°C, which moved to the right of the main peak position nearby 2 nm, and the peak intensity increased. The sample had abundant mesopores at 850°C, which the content and pore diameter had expanding tendency; this result is consistent with the data in Table 2. The 850°C

Table 2. Specific surface area, pore volume, and aperture parameters of wooden activated carbon fibers (WACF) and Mn/TiO_2-WACF at different calcination temperatures.

Sample	S_{BET} ($m^2\ g^{-1}$)	S_{mic} ($m^2\ g^{-1}$)	S_{meso} ($m^2\ g^{-1}$)	Vtot ($cm^3\ g^{-1}$)	Vmic ($cm^3\ g^{-1}$)	Vmeso ($cm^3\ g^{-1}$)	Vmic/Vmeso	Pore radius (nm)
WACF	1741.8	1272.1	530.3	0.846	0.581	0.294	1.98	1.94
450°C	1238.7	803.2	322.4	0.628	0.364	0.230	1.58	2.03
550°C	1427.5	935.9	354.5	0.709	0.428	0.235	1.82	1.99
650°C	1788.4	1156.4	467.2	0.909	0.529	0.335	1.58	2.03
750°C	1094.6	579.0	365.0	0.542	0.260	0.231	1.12	1.98
850°C	1477.7	547.6	1249.7	0.734	0.230	0.732	0.31	1.99

Note: S_{BET}, BET surface area; S_{mic}, micropore surface area; S_{meso}, mesopore surface area; V_{tot}, total pore volume; V_{mic}, micropore volume; V_{meso}, mesopore volume.

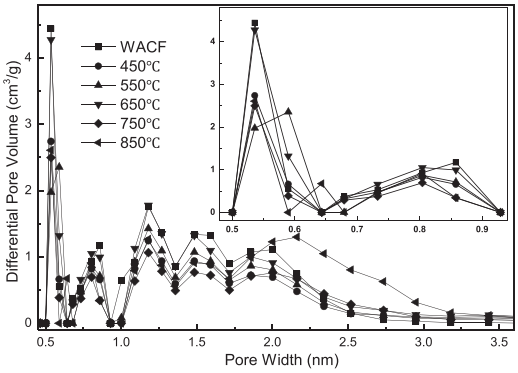

Figure 5. Pore size distribution of the wooden activated carbon fibers (WACF) and Mn/TiO_2-WACF under different calcination temperatures (DFT method).

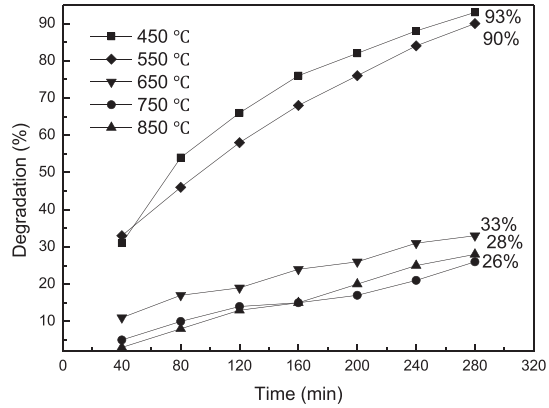

Figure 6. Degradation curve chart of the samples with methylene blue under visible lights.

calcination temperature was higher than the activation temperature (800°C) of the WACF, and the second calcination of the 850°C sample was equivalent to the second WACF activation.

Degradation Performance under Visible Lights

To study the degradation performance under visible lights of the Mn/TiO_2-WACF prepared at different calcination temperatures, methylene blue solution was selected as a model in conducting a photocatalysis degradation experiment. Figure 6 shows the visible light degradation curves of the methylene blue solution with varying illumination time. The methylene solution degradation by Mn/TiO_2-WACF sample under visible lights gradually decreased with the increase of calcination temperature mainly because the TiO_2 crystal transformed from anatase into rutile phase as calcination temperature increased. In addition, after reacting for 280 min, the methylene blue solution visible light degradation rate by 850°C sample was higher than that by the 750°C sample because the calcination temperature influenced the pore structure of the carrier material WACF.

CONCLUSIONS

Phase change occurred in the Mn/TiO_2-WACF-loaded TiO_2 within 650-750°C calcination temperature. Mn doping elevated the phase change temperature of the TiO_2 in the sample. The particle size of the anatase TiO_2 in the sample gradually enlarged with the increase of calcination temperature. The Ti–O–C bond adsorption peak in the Mn/TiO_2-WACF IR spectrum initially increased and then decreased with the increase of calcination temperature, and the calcination temperature at 750°C became a turning point of the variations of this adsorption peak. The N_2 adsorption capacity of the Mn/TiO_2-WACF sample gradually increased under 650°C with the increase of calcination temperature, which abruptly decreased when temperature increased to 750°C. The degradation of the methylene blue solution by Mn/TiO_2-WACF sample gradually decreased with the increase of calcination temperature, and the degradability of the sample obtained at 450°C was superior.

ACKNOWLEDGMENTS

This research was financially supported by National Natural Science Foundation of People's Republic of China (No. 31270607).

REFERENCES

Baban A, Yediler A, Liene RD (2003) Ozonation of high strength segregated effluents from awoollen textile dyeing and fmishing plant. Dyes Pigments 58(2):93-98.

Chen X, Mao SS (2007) Titanium dioxide nanomaterials: Synthesis, properties, modifications, and applications. ChemInform 107(7):2891-2959.

Fox MA, Dulay MT (1993) Heterogeneous photocatalysis. Chem Rev 93(1):341-357.

Fu PF, Luan Y, Dai XG (2004) Preparation of activated carbon fibers supported TiO_2 photocatalyst and evaluation of its photocatalytic reactivity. J Mol Catal Chem 221(1):81-88.

Gong Q, Hu Y, Wei CH, Zhang X (2012) Study on the photocatalytic properties of Mn, N-doped TiO_2 prepared at different calcination temperatures. Acta Scientiae Circumstantiae 32(4):803-805.

Li DN, Ma XJ (2013) Effect of activation technology on wooden active carbon fiber structure and iodine adsorption property. J Funct Mater 44(17):2565-2769.

Li FX, Lu XH, Mei P (2006) Progress in research on effects of metal ion dopants on crystal phase transformation of TiO_2. Mater Rev 20(9):13-16.

Li PG, Bono A, Krishnaiah D, Collin JG (2008) Preparation of titanium dioxide photocatalyst loaded onto activated carbon support using chemical vapor deposition: A review paper. J Hazard Mater 157:209-219.

Ma X, Liu X, Yu L, Tian M (2014a) The microstructure and adsorption property of bamboo based activated carbon fibers prepared by liquefaction and curing. Wood Fiber Sci 46(2):291-299.

Ma X, Zhang F, Zhu J, Yu L, Liu X (2014b) Preparation of highly developed mesoporous activated carbon fiber from liquefied wood using wood charcoal as additive and its adsorption of methylene blue from solution. Biores Technol 164(1):1-6.

Naeem K, Feng O (2010) Preparation of Fe3+-doped TiO_2 nanoparticles and its photo catalytic activity under UV light. Physica B 405(1):221-226.

Subramanian M, Vuayalakshmi S, Venkataraj S, Jayavel R (2008) Effect of cobalt doping on the structural and optical properties of TiO_2 films prepared by sol-gel process. Thin Solid Films 516(12):3776-3782.

Tanaka K, Padermpole K, Hisanaga T (2000) Photocatalytic degradation of commercial azo dyes. Water Res 34(1): 327-333.

Wang Q, Jiang ZY, Wang YB, Chen DM, Yang D (2009) Photocatalytic properties of porous C-doped TiO_2 and Ag/C doped TiO_2 nanomaterials by eggshell membrane templating. J Nanopart Res 11(2):375-384.